MINERALOGICAL MAGAZINE

JOURNAL OF THE MINERALOGICAL SOCIETY

Vol. 35 December 1965 No. 272

The mineralogy of metamorphosed basic rocks from the Willyama Complex, Broken Hill district, New South Wales. Part II. Pyroxenes, garnets, plagioclases, and opaque oxides

(With Plates VIII and IX)

By R. A. Binns, B.Sc., Ph.D.,

Department of Geology, University of New England, Armidale, N.S.W.

[Read 23 September 1965]

Summary. Chemical and optical data are presented for the orthopyroxenes, clinopyroxenes, garnets, plagioclases, and opaque oxides in high-grade regionally metamorphosed basic rocks and their garnetiferous associates from the Willyama Complex. Exsolution phenomena in the pyroxenes have been studied by X-ray diffraction methods and with the electron probe micro-analyser. The (001) lamellae in one lime-rich clinopyroxene are clinohypersthene. Comparison of the Willyama and other granulite facies clinopyroxenes with those of slowly cooled basic igneous rocks suggests that their chemical compositions may be used as guides to temperature conditions during formation. Willyama plagioclases are complexly twinned and possess intermediate structural states.

IN Part I (Binns, 1965) attention has been drawn to grade-dependent changes in the chemical composition of hornblendes in metamorphosed basic rocks and their garnetiferous associates from the three zones of progressive regional metamorphism in the Precambrian Willyama Complex of New South Wales. This part is devoted to the other minerals of these rocks. To facilitate comparison of coexisting phases, minerals are identified by the number of their host rock with a prefix to indicate the species. Thus H26, G26, C26, and P26 denote hornblende, garnet, clinopyroxene, and plagioclase respectively from specimen 26. Details of the numbering, localities, and petrographical information for the host rocks are provided by Binns (1964, appendix I). Certain aspects of some Willyama pyroxenes have been discussed previously (Binns, 1962).

Analysed mineral concentrates were separated using a combination of magnetic and heavy liquid techniques, a purity in excess of 99 % being achieved in all cases except certain plagioclases and opaque oxides. Garnet concentrates free of inclusions (better than 99·5 % pure) were obtained by first separating relatively coarse-grained material (90–150 mesh), then crushing the resulting concentrate to pass through a 200-mesh sieve and repeating the heavy liquid separation after removing dust by elutriation. During separation of hornblendes, pyroxenes, and garnets, almost the entire concentrate sank or floated within a very restricted density interval (approximately 0·005), confirming the lack of compositional zoning indicated by refractive-index measurements.

All chemical analyses listed in this paper were performed by the author in the Department of Mineralogy and Petrology, Cambridge, using conventional analytical techniques. Ferrous iron was determined by the ammonium-vanadate method (Wilson, 1955). Care was taken during analysis of garnets to minimize attack on platinum ware caused by high manganese content, but as a precaution against possible dissolved platinum, the R_2O_3 precipitations for garnets and orthopyroxenes were preceded by acid H_2S precipitations.

Refractive indices were determined on grains from the analysed concentrates or, where necessary, on oriented grains plucked from thin sections. Optic axial angles were measured conoscopically (pyroxenes) or orthoscopically (plagioclases) on grains for which both optic axes were accessible. Densities were measured by the method described in Part I.

Clinopyroxene

In Zone B, lime-rich clinopyroxene is restricted to relatively calcic amphibolites (e.g. specimen 26 with 13·8 % CaO). It is a common constituent of basic gneisses from Zone C, and occurs also in lime-rich rocks included within or developed at the margins of basic gneisses.

Optical and physical properties. In hand specimens and mineral crushes Willyama clinopyroxenes are greyish-green in colour. Most are colourless in thin section, but particularly iron-rich varieties are pale green and faintly pleochroic.

The refractive indices and densities of the analysed clinopyroxenes increase with content of iron (table I, fig. 1). The range in composition of Zone C clinopyroxenes is indicated by the variation in β refractive index, from 1·692 to 1·725, of some fifty samples. Except for C5, where exsolution has apparently affected 2V, optic axial angles conform to values predicted from the diagrams of Hess (1949).

Two kinds of exsolution lamellae are present in Zone C clinopyroxenes (pl. VIII*a*). One set, consisting of relatively evenly spaced sheets

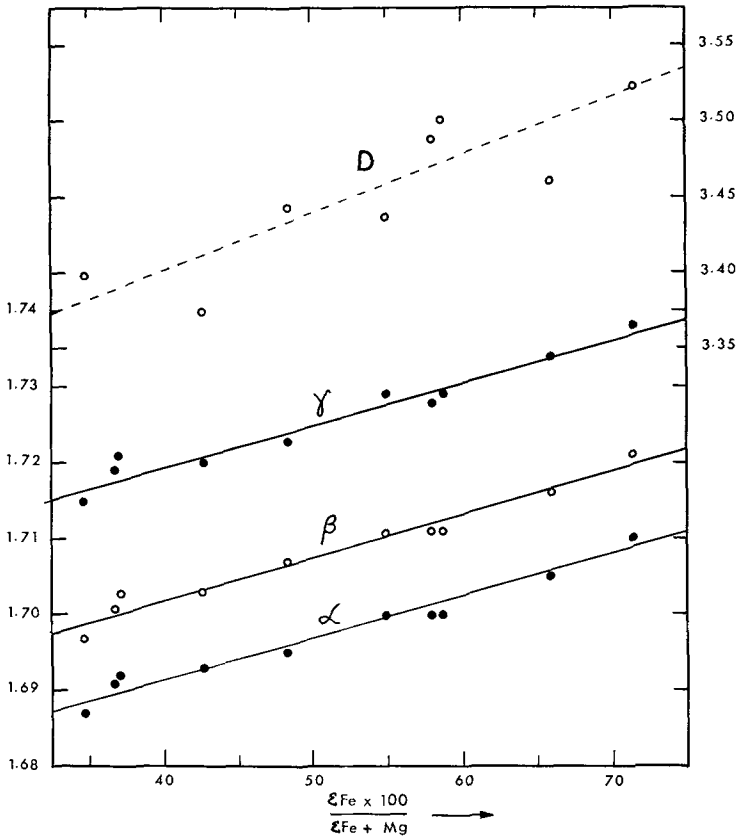

FIG. 1. Variation in refractive indices and density of Willyama clinopyroxenes with iron content.

parallel to (001) of the host, up to 4μ thick, occurs in all Zone C clinopyroxenes examined, most abundantly in iron-rich varieties. The second set, restricted to iron-rich clinopyroxenes that coexist with orthopyroxene (i.e. clinopyroxenes relatively poor in calcium), consists of very narrow closely spaced sheets parallel to (100) of the host. Under very high magnification, especially in (010) sections, some of the latter are finely crenulated.

Well-developed exsolution lamellae of both types were studied in

detail in clinopyroxene C5. Single crystal X-ray oscillation photographs (method of Bown and Gay, 1959) possess, superimposed on the $C2/c$ clinopyroxene pattern of the host phase, spots due both to homoaxial orthopyroxene and to a $P2_1/c$ clinopyroxene oriented with a and b coincident with the host and c inclined at 3° to that of the host in acute β of the latter (pl. IX*b*). Photographs of clinopyroxene C2, which has only (001) lamellae, lack the subsidiary orthopyroxene spots, thereby identifying the (100) lamellae in C5 as orthopyroxene and the (001) lamellae as a pigeonite-type clinopyroxene.

The (100) orthopyroxene lamellae have higher refractive indices and lower birefringence than the host clinopyroxene. Although they are too thin to allow accurate measurement, their extinction angle is clearly very different from that of the host. The (001) lamellae are pale smoky brown in colour and apparently non-pleochroic. Under very high magnification they show fine-scale polysynthetic twinning with (100) as composition plane, but one of the twin sets is subordinate and gives rise to no corresponding spots on X-ray photographs. Refractive indices listed in table II, measured on lamellae in (100) and (010) clinopyroxene sections plucked from a thin slice of half the normal thickness, indicate a very low optic axial angle.

Traverses with the electron probe micro-analyser across a grain of clinopyroxene C5 sectioned approximately parallel to (100) (pl. IX*a*) are illustrated in fig. 2 (see also Binns, Long, and Reed, 1963). This grain possesses (001) lamellae of pigeonite-type clinopyroxene from 1 to 4μ thick, spaced on the average at 40-micron intervals. Measurements of Ca-K_α, Fe-K_α, and Mg-K_α radiation over the thicker lamellae permit calculation of their chemical composition (table II). There is a significant discrepancy between the ratio Fe/(Fe+Mg) obtained with the micro-analyser and that estimated by comparison of lamellae refractive indices with the synthetic data of Bowen and Schairer (1935), possibly due to the influence of other components in the lamellae. An interesting feature of the profiles in fig. 2 is the suggestion of slight calcium enrichment and iron depletion in the host clinopyroxene adjacent to the calcium-poor lamellae.

The very low calcium content of the (001) lamellae in clinopyroxene C5 (less than 0·5 wt % CaO) makes them members of the clinoenstatite–clinoferrosilite mineral series rather than pigeonites. Clinohypersthene (previously regarded as pigeonite) has also been identified as (001) lamellae in an igneous augite from the Bushveld Complex (Binns, Long, and Reed, 1963). These are the first terrestrial occurrences of clino-

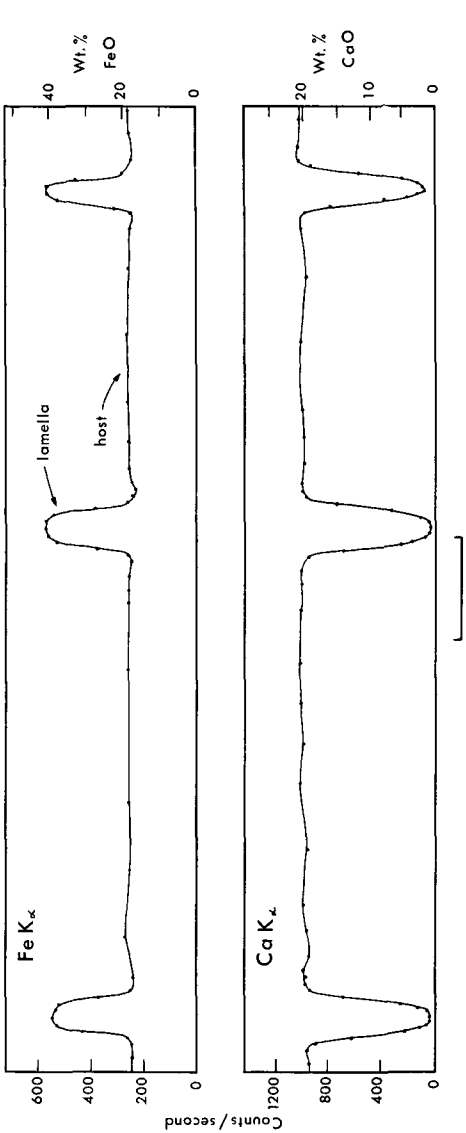

FIG. 2. Profiles of iron and calcium composition across the lamellate clinopyroxene grain illustrated on pl. IX, obtained with the electron-probe micro-analyser. Traverses were made using a manually operated step scanner, from 3000 to 10 000 pulses being counted at each point shown on the figure. Corrections were applied for background radiation. The sloping 'edge effect' at lamellae boundaries is due to limited resolution of the electron probe and to fluorescence effects.

TABLE I. Chemical analyses, cation contents, and optical and physical properties of Willyama clinopyroxenes. Analyst: R. A. Binns. Localities and petrography of host rocks given in Appendix 1, Binns (1964)

	Zone C									Zone B
	C1	C2	C3	C4	C5	C6	C7	C8	C10	C26
SiO_2	51·03	51·05	49·15	51·68	50·47	50·95	50·65	48·60	49·66	50·20
TiO_2	0·20	0·25	0·40	0·39	0·39	0·25	0·28	0·38	0·34	0·27
Al_2O_3	2·12	1·16	1·47	1·44	1·24	2·40	3·14	1·84	2·03	1·27
Fe_2O_3	0·75	0·10	1·28	0·55	0·66	0·63	0·26	1·17	1·22	0·75
FeO	13·08	15·67	21·39	11·32	18·21	11·70	11·85	21·68	17·74	16·82
MnO	0·49	0·38	0·82	0·26	0·32	0·33	0·26	0·38	0·25	1·11
MgO	10·73	9·66	6·82	12·70	8·86	12·09	11·81	5·23	7·54	7·54
CaO	21·28	21·49	19·09	21·54	20·04	20·90	21·30	20·43	21·34	22·31
Na_2O	0·39	0·24	0·36	0·30	0·16	0·42	0·40	0·31	0·38	0·29
K_2O	0·02	0·01	0·03	0·01	0·01	0·01	0·03	0·04	0·00	0·01
H_2O^-	0·00	0·00	0·00	0·00	0·00	0·00	0·00	0·00	0·00	0·00
Total	100·09	100·01	100·81	100·19	100·36	99·68	99·98	100·06	100·50	100·57
Cation contents to six oxygen atoms and $Z = 2·00$										
Si	1·943	1·968	1·933	1·949	1·956	1·932	1·916	1·936	1·935	1·952
Al^{iv}	0·057	0·032	0·067	0·051	0·044	0·068	0·084	0·064	0·065	0·048
Al^{vi}	0·038	0·019	0·002	0·012	0·012	0·042	0·057	0·022	0·028	0·010
Ti	0·005	0·007	0·012	0·011	0·012	0·007	0·008	0·012	0·010	0·008
Fe'''	0·021	0·003	0·038	0·016	0·019	0·018	0·009	0·035	0·035	0·022
Fe''	0·416	0·505	0·704	0·358	0·591	0·372	0·375	0·722	0·574	0·547
Mn	0·016	0·012	0·028	0·007	0·012	0·011	0·008	0·012	0·008	0·037
Mg	0·608	0·556	0·399	0·714	0·510	0·684	0·666	0·308	0·435	0·437
Ca	0·868	0·887	0·803	0·870	0·834	0·851	0·864	0·872	0·885	0·929
Na	0·027	0·018	0·028	0·023	0·014	0·032	0·032	0·024	0·028	0·022
K	0·001	0·000	0·001	0·000	0·000	0·000	0·001	0·002	0·000	0·000

TABLE I (*cont.*)

	Zone C									Zone B
	C1	C2	C3	C4	C5	C6	C7	C8	C10	C26
$\Sigma(X+Y)$	2·000	2·007	2·015	2·011	2·004	2·017	2·020	2·009	2·003	2·012
Ca	45·0	45·2	41·0	44·3	42·4	44·0	45·0	44·8	45·7	47·1
Mg	31·5	28·2	20·0	36·3	26·0	35·3	34·7	15·8	22·5	22·2
ΣFe	23·5	26·6	39·0	19·4	31·6	20·7	20·3	39·4	31·8	30·7
$100\Sigma Fe/(Mg+\Sigma Fe)$	42·7	48·4	65·9	34·8	54·9	36·9	37·1	71·5	58·7	58·1
Optical and physical properties										
α	1·693	1·695	1·705	1·687	1·700	1·691	1·692	1·710	1·700	1·700
β	1·703	1·707	1·716	1·697	1·711	1·701	1·703	1·721	1·711	1·711
γ	1·720	1·723	1·734	1·715	1·729	1·719	1·721	1·738	1·729	1·728
Δ	0·027	0·028	0·029	0·028	0·029	0·028	0·029	0·028	0·029	0·028
$2V_\gamma$	55°	57°	54°	52°	49°	52°	53°	60°	61°	58°
γ: [001]	43°	43°	43°	43°	42°	42°	43°	45°	45°	44°
D (gm/cc)	3·375 ±0·006	3·444 ±0·003	3·46 ±0·02	3·399 ±0·003	3·437 ±0·001	—	—	3·522 ±0·002	3·503 ±0·004	3·488 ±0·005
*Development of exsolution lamellae**										
//(001)	s	m	s	s	s	m	x	s	p	a
//(100)	p	a	s	m	s	p	p	m	a	a

* s = strongly developed; m = moderately well developed; p = poorly developed; a = absent; x = present but altered.

hypersthene to be verified by analytical data. However, the possibility that clinohypersthene occurs in pyroxene intergrowths was earlier suggested by Henry (1938).

TABLE II. Chemical composition and optical properties of clinohypersthene occurring as lamellae in clinopyroxene C5

Electron probe analysis (wt %)		Calculated composition (wt %)*		Cation contents to six oxygen atoms		Optical properties	
Fe	31·8	SiO_2	49·8	Si	2·00	α	1·740±0·005
Mg	6·3	FeO	40·9	Fe″	1·37	β	1·740±0·005
Ca	tr.†	MgO	10·5	Mg	0·63	γ	1·765±0·005
		CaO	tr.‡	Ca	0·00	γ: [001] 38° in obtuse β	
		Total	101·2				

* Composition obtained by allotting silicon and oxygen according to a metasilicate formula.

† Less than 0·4 wt % Ca.

‡ Less than 0·5 wt % CaO.

Textural relationships in Willyama Complex metabasic rocks (cf. Binns, 1964, figs. 6, 7) show that the clinopyroxenes from which clinohypersthene lamellae have exsolved originally crystallized (under granulite facies conditions of metamorphism) in equilibrium with orthopyroxene rather than pigeonite. Clinohypersthene evidently separated from lime-rich clinopyroxene below the temperature where orthopyroxene (hypersthene) is the stable calcium-poor pyroxene phase. Similar situations in igneous rocks were described by Bown and Gay (1960) and Best (1963). These relationships and recent experimental studies of $MgSiO_3$ polymorphism (reviewed by Boyd and Schairer, 1964) invalidate the method of estimating crystallization temperature by applying Bowen and Schairer's (1935) orthopyroxene–clinopyroxene inversion relationships to exsolution lamellae in pyroxenes (cf. Hess, 1960).

Chemistry. Analyses and cation contents of nine clinopyroxenes from Zone C and one from Zone B (C26) are presented in table I. All are essentially metasilicates of calcium, iron, and magnesium and their composition can be represented accurately on a triangular plot of these three components (fig. 3*a*).

The low aluminium contents of Willyama clinopyroxenes parallel similar deficiencies in coexisting orthopyroxenes. Most of the aluminium in both pyroxene groups replaces silicon in the *Z* sites. Alkali contents of the Willyama clinopyroxenes are also low, soda reaching a maximum

of only 0·42 wt % in C6. In all cases there is sufficient ferric iron and octahedrally co-ordinated aluminium to balance sodium as acmite–jadeite molecule.

Titanium and manganese are minor components of the analysed clinopyroxenes. The latter attains relatively high values in iron-rich clinopyroxene C3 and in clinopyroxene C26, which coexists with almandine garnet (G26, table IV).

Fig. 3*a* shows that Willyama clinopyroxenes coexisting with orthopyroxene describe a trend of decreasing calcium content (increasing 'solid solution of orthopyroxene') with increasing iron content. The three clinopyroxenes that do not coexist with orthopyroxene (C8, C10, C26) lie well to the calcium-rich side of this trend. A tendency for solid solution between orthopyroxene and clinopyroxene to increase with grade across Zone C has been noted previously (Binns, 1962, fig. 5).

If attention is restricted to clinopyroxenes that coexist with calcium-poor pyroxene (i.e. to those probably saturated with orthopyroxene), there is a significant difference between the trends of metamorphic and plutonic igneous clinopyroxenes on a Ca–Mg–ΣFe plot (fig. 3*b*) indicating restriction of the immiscibility field between lime-rich and lime-poor pyroxenes at the higher temperatures of igneous rocks. Such a temperature-dependent relationship has been demonstrated experimentally for magnesian pyroxenes (Atlas, 1952; Boyd and Schairer, 1964). Fig. 3 reveals that the change in the solvus is accentuated in iron-rich pyroxenes, suggesting that the calcium contents of natural coexisting pyroxenes might prove useful indicators of crystallization temperatures. Experiments by Davis (1963) show that the shape of the solvus for magnesian pyroxenes is essentially independent of variations in pressure.

Orthopyroxene

Calcium-poor orthopyroxene is an abundant constituent of basic rocks in Zone C, the highest-grade zone in the Willyama Complex. It also occurs in garnet- and biotite-bearing assemblages found at the boundaries between certain Zone C basic rocks and gneisses of pelitic or quartzo-feldspathic composition (cf. Binns, 1964, fig. 10). However, orthopyroxene-bearing charnockitic rocks are unknown in the Willyama Complex.

Optical and physical properties. Orthopyroxene concentrates are yellowish-green to khaki in colour. In thin section some show faint pleochroism from pale pink to pale green but most are almost colourless. Although orthopyroxene O16 is anomalous, the chemical data and

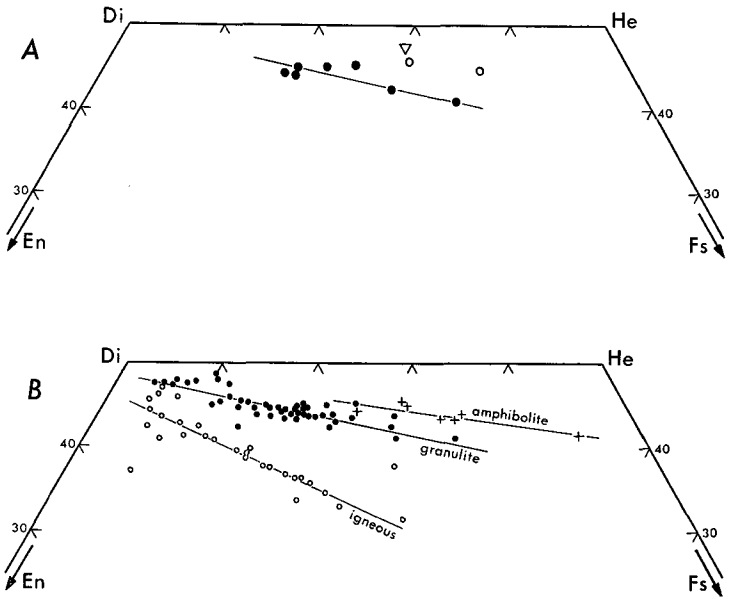

FIG. 3. *a*. Portion of the pyroxene quadrilateral on a triangular Ca–Mg–ΣFe plot showing Willyama clinopyroxenes that coexist with orthopyroxene in Zone C (solid circles), Zone C clinopyroxenes that do not coexist with orthopyroxene (open circles), and a clinopyroxene from a Zone B garnetiferous amphibolite (open triangle).

b. A similar plot showing clinopyroxenes that crystallized with coexisting lime-poor pyroxene (orthopyroxene or pigeonite) in various environments. Clinopyroxenes from slowly cooled igneous rocks (peridotites, gabbros, dolerites, or diorites) are denoted by open circles (sources of data: Best, 1963; Brown, 1956, 1957; Green, 1964; Hess, 1949, 1960; McDougall, 1961; Muir, 1954); metamorphic clinopyroxenes from granulite-facies gneisses by solid circles (data: this paper; Clavan, McNabb and Watson, 1954; Engel, Engel, and Havens, 1964; Eskola, 1952; Green, 1964; Howie, 1955, 1958, 1964*a*, 1964*b*; O'Hara, 1960, 1961; Philipsborn, 1930; Subramaniam, 1962); and amphibolite-facies clinopyroxenes (from rocks in which the coexisting orthopyroxene was probably derived by a process other than the breakdown of aluminous hornblende) by crosses (Kranck, 1961). There is a clear difference between igneous and metamorphic clinopyroxenes that coexist with orthopyroxene, and a somewhat less distinct separation of granulite- from amphibolite-facies clinopyroxenes that nevertheless conforms to the progressive restriction of the miscibility gap between lime-rich and lime-poor pyroxenes with increase in temperature of formation. Certain clinopyroxenes from volcanic rocks fall below the igneous trend shown on the figure, but in view of possible metastable crystallization under conditions of rapid cooling, volcanic clinopyroxenes have not been included with those from slowly cooled igneous rocks.

absorption colours listed in table III support the conclusion of Howie (1963) that orthopyroxene pleochroism depends on aluminium content. No correlation can be detected between depth of pleochroism and content of iron, manganese, or titanium, or of the trace constituents nickel

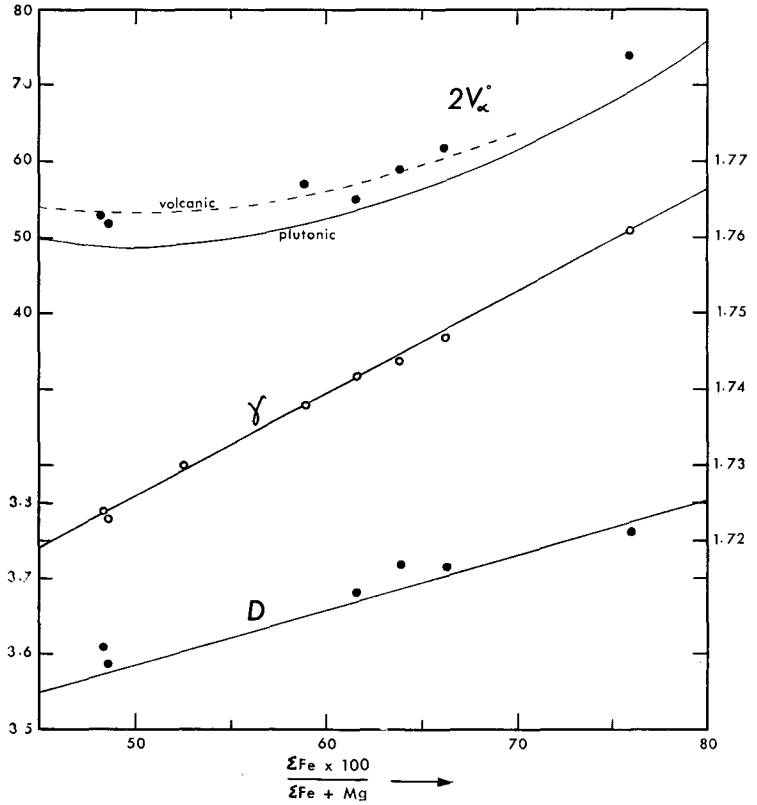

FIG. 4. Variation in γ refractive index, optic axial angle, and density with composition in Willyama orthopyroxenes. The curves for optic axial angles of 'plutonic' and 'volcanic' orthopyroxenes are taken from Hess (1952).

and chromium.[1] The delicate pearly-mauve colour of O4 and O5, seen only in thick grain mounts, may denote the presence of trivalent titanium.

The relationship between γ refractive indices and iron-magnesium ratio of the Willyama orthopyroxenes is illustrated on fig. 4. The

[1] Trace element data for Willyama minerals will be published separately.

γ refractive index for over seventy specimens ranges from 1·720 to 1·766. Again, no zoning is evident. Optic axial angles are consistently slightly higher than those of 'plutonic' orthopyroxenes of comparable iron content (see fig. 4). Density also increases regularly with iron content.

The Willyama orthopyroxenes possess fine plate-like exsolution lamellae parallel to (100) (pl. VIII*b*). Best seen in (010) sections, these exist with two optic orientations, extinguishing symmetrically at angles between 20° and 40° either side of the (100) symmetry plane of the host. Single crystal X-ray patterns (cf. Bown and Gay, 1959) identify the lamellae as clinopyroxene of the 'augite type' (space group $C2/c$), occurring in structural alignment with the host orthopyroxene (c and b crystallographic axes common, a axes of clinopyroxene inclined on either side of the common (100) plane in a 'twin-like arrangement' and varying between the two extreme conditions where the lamellae favour one orientation exclusively or the two equally). Such lamellae have been observed in all Willyama orthopyroxenes, but are most abundant in iron-rich specimens that coexist with clinopyroxene (i.e. those with highest overall calcium contents). Their abundance suggests that ordering into calcium-rich and calcium-poor phases has been particularly thorough.

Chemistry. Seven complete analyses and one partial analysis of orthopyroxene are presented in table III. All coexist with clinopyroxene, except O16 from a garnet-bearing rock at the margin of a basic gneiss body.

Replacement of magnesium by iron is extensive. Orthopyroxene O3, from an iron-rich pod of intermediate composition (52·7 % SiO_2) within basic gneiss, contains 76 mol % ferrosilite. Manganese is a significant component, varying in sympathy with the amount in host rocks and in coexisting minerals.

Calcium content is low, tending to increase with iron content in those orthopyroxenes bound to the pyroxene solvus through coexistence with lime-rich clinopyroxene. Orthopyroxene O16 contains slightly less calcium than those of comparable iron content coexisting with clinopyroxene. The higher calcium contents of orthopyroxenes from the higher grade portions of Zone C (Binns, 1962, fig. 5) accord with an increase in solid solution between calcium-rich and calcium-poor pyroxenes at higher temperatures. However, although such a tendency is emphasized by the more calcic orthopyroxenes of igneous rocks, the variations in calcium content are considerably smaller than in coexisting

TABLE III. Chemical analyses, cation contents, and optical and physical properties of Willyama orthopyroxenes (Zone C). Analyst: R. A. Binns

	O1	O2	O3	O4	O5	O6	O7	O16
SiO_2	49·34	49·27	47·44	51·13	49·04	50·26	n.d.	48·78
TiO_2	0·18	0·28	0·48	0·29	0·24	0·21	n.d.	0·29
Al_2O_3	1·28	0·23	0·92	0·87	0·89	2·05	n.d.	2·10
Fe_2O_3	0·60	0·09	0·32	0·67	0·57	0·63	1·78	0·37
FeO	32·83	36·55	40·75	28·22	36·86	28·30	28·34	34·59
MnO	1·26	0·87	1·64	0·61	0·72	0·80	0·84	0·98
MgO	13·51	11·98	7·63	17·51	10·88	17·28	15·56	12·68
CaO	0·87	0·82	1·10	0·95	1·36	0·87	0·87	0·80
Na_2O	0·13	0·03	0·21	0·04	0·03	0·03	n.d.	n.d.
K_2O	0·04	0·01	0·02	0·01	0·01	0·01	n.d.	n.d.
H_2O^-	0·00	0·00	0·00	0·02	0·00	0·00	n.d.	0·00
Total	100·04	100·13	100·51	100·32	100·60	100·44	—	100·59
Cation contents to six oxygen atoms and Z = 2·00								
Si	1·952	1·976	1·952	1·962	1·964	1·931		1·930
Al^{iv}	0·048	0·010	0·044	0·038	0·036	0·069		0·070
Al^{vi}	0·014	0·000	0·000	0·003	0·007	0·023		0·028
Ti	0·005	0·010	0·015	0·009	0·007	0·006		0·008
Fe‴	0·019	0·002	0·010	0·018	0·017	0·018		0·011
Fe″	1·087	1·226	1·401	0·904	1·235	0·910		1·143
Mn	0·043	0·029	0·057	0·021	0·024	0·025		0·033
Mg	0·797	0·716	0·467	1·001	0·650	0·988		0·746
Ca	0·036	0·036	0·047	0·039	0·058	0·036		0·033
Na	0·005	0·001	0·017	0·004	0·003	0·002		—
K	0·002	0·000	0·000	0·000	0·000	0·000		—
$\Sigma(X+Y)$	2·008	2·020*	2·014†	1·999	2·001	2·008		2·002
Ca	1·9	1·8	2·4	2·0	2·9	1·8	1·9	1·7
Mg	40·2	35·6	23·6	50·4	32·8	50·0	46·6	37·9
ΣFe	57·9	62·6	74·0	47·6	64·3	48·2	51·5	60·4
$100\Sigma Fe/(Mg+\Sigma Fe)$	58·9	63·8	75·9	48·6	66·2	48·4	52·5	61·6
Optical and physical properties								
Colour								
$//\alpha$	colourless	colourless	pale pink	v. pale mauve	colourless	pale pink	pale pink	pale pink
$//\gamma$	colourless	colourless	pale apple green	faintly pearly	v. faint pearly-mauve	pale grey-green	pale grey-green	pale grey-green
γ (±0·001)	1·738	1·744	1·761	1·723	1·747	1·724	1·730	1·742
$2V_\alpha$	57°	59°	74°	52°	62°	53°	—	55°
D(gm/cc)	—	3·720	3·761	3·589	3·716	3·61	—	3·684
	—	±0·003	±0·007	±0·002	±0·002	±0·01	—	±0·005

* Z = 1·986. † Z = 1·996.

clinopyroxenes and may be more susceptible to the influence of other components.

There is little aluminium in the analysed Willyama orthopyroxenes, apart from O16, which coexists with garnet. Although aluminium is absent from analyses of charnockite orthopyroxenes from south-western Finland listed by Parras (1958), high aluminium contents are often reported in granulite facies and charnockitic orthopyroxenes. They have been correlated by Eskola (1957) with high-pressure environments

of formation, for which there is some support in the experimental studies of Boyd and England (1960). The Willyama data, however, indicate that aluminium contents of isogradal pyroxenes depend very much upon host-rock chemistry and the nature of coexisting phases. There is some suggestion that the more aluminous pyroxenes coexist with more sodic plagioclases, and the low aluminium contents of Willyama pyroxenes compared to those from certain other metamorphic terrains may reflect the relatively low sodium contents of their host rocks rather than differences in pressure conditions. Since mineralogical evidence of alumina-saturation is rare in orthopyroxene-bearing metamorphic rocks, great caution is required when applying the experimental results of Boyd and England.

In orthopyroxenes O2 and O3, aluminium is not quite sufficient to make up the deficiency of silicon in the *Z* sites, but this may simply be due to small analytical errors and the method of computing cation contents. The amount of aluminium apparently entering the *Y* sites of orthopyroxenes O1, O4, and O5 is very small and little significance can be attached to the figures quoted in table III.

Titanium, ferric iron, and sodium are only minor constituents in the Willyama orthopyroxenes. Potassium is virtually absent.

The wide range in iron content shown by orthopyroxene when it first appears with increasing metamorphic grade as a product of hornblende breakdown in metamorphosed basic rocks makes the orthopyroxene isograd a very practical zonal boundary. Refractive indices of specimens from close to the orthopyroxene isograd dividing Zone B from Zone C vary over the entire range observed for the whole of Zone C, so that the temperature at which hornblende commences to break down yielding, *inter alia*, orthopyroxene appears comparatively insensitive to iron-magnesium ratios of the host rocks. This conclusion may not hold true for extremely iron-rich or magnesium-rich rocks such as are not found in the Willyama Complex.

Garnet

Although not a constituent of metamorphosed basic rocks *sensu stricto*, garnet is found in hornblende- and pyroxene-bearing assemblages occurring within or at the margins of basic gneisses and amphibolites. The chemical composition of garnetiferous assemblages varies considerably (see Binns, 1964, table III), but all are characterized by a high iron to magnesium ratio. Except for some cases where there is not sufficient aluminium available to combine with iron to form garnet,

the ratio Fe/(Fe+Mg) = 0·65 roughly divides garnetiferous from non-garnetiferous basic assemblages. Many garnet-bearing assemblages contain free quartz. Few contain normative corundum, and on a standard ACF diagram garnetiferous assemblages generally fall no closer to the alumina apex than non-garnetiferous basic gneisses or

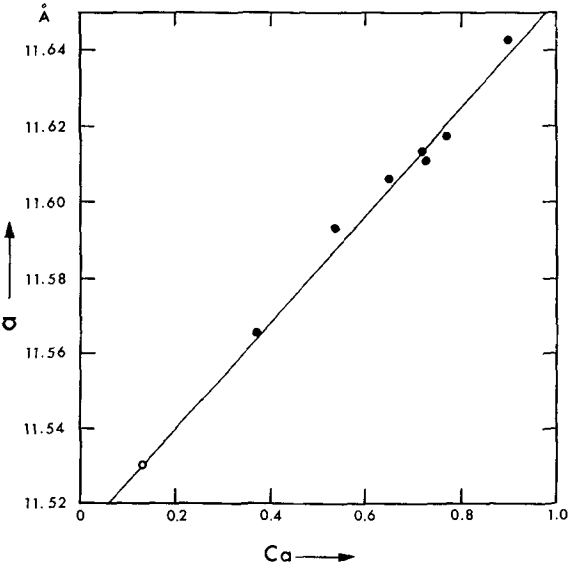

FIG. 5. Dependence of cell dimensions upon grossular content (expressed as atoms of calcium per twelve oxygens) in Willyama garnets. Solid circles, garnets from rocks of metabasic association; open circle, garnet from a pelitic gneiss.

amphibolites. Consequently iron rather than aluminium is the critical component controlling occurrence of garnet, and in the paragenetic analysis of garnetiferous assemblages iron and magnesium must be considered apart. No anomaly then exists in the occurrence together (in Zone C) of clinopyroxene–garnet–plagioclase–quartz and orthopyroxene–plagioclase–quartz assemblages.

Optical and physical properties. With the exception of G16 (with the lowest grossular content and possessing the lilac tint more typical of garnets in Willyama pelitic rocks), the garnets listed in table IV are buff-pink in colour. Measured refractive indices, densities, and cell dimensions compare favourably with values calculated from the analytical data by assuming linear compositional variation of optical and physical properties between those of synthetic end-member garnets

(Skinner, 1956). Density and refractive index are dominated by the almandine component; both are reduced by the presence of pyrope and grossular but are little affected by variation in spessartine. Variation in unit cell edges is influenced mainly by grossular content, as illustrated in fig. 5.

TABLE IV. Chemical analyses, cation contents, and properties of Willyama garnets. Analyst: R. A. Binns

	Zone C			Zone B		Zone A	
	G10	G16	G17	G26	G28	G36	G40
SiO_2	36·98	36·19	36·95	37·03	36·79	36·44	36·14
TiO_2	0·10	0·21	0·15	0·25	0·20	0·36	0·49
Al_2O_3	20·93	22·26	20·48	21·11	21·31	21·15	21·09
Fe_2O_3	1·08	1·51	0·96	0·00	0·40	0·68	1·06
FeO	29·55	29·89	28·32	26·53	28·45	29·18	22·32
MnO	1·25	2·89	3·52	5·92	4·78	2·86	8·16
MgO	1·85	3·42	2·00	1·60	1·96	0·92	0·96
CaO	8·57	4·35	7·61	8·48	6·33	8·93	10·05
Total	100·31	100·72	99·99	100·92	100·22	100·52	100·27
Cation contents to 12 oxygen atoms							
Si	2·96	2·89	2·97	2·96	2·95	2·93	2·90
Al	1·97	2·09	1·94	1·98	2·01	2·00	1·99
Ti	0·00	0·01	0·01	0·01	0·01	0·02	0·03
Fe‴	0·06	0·09	0·06	0·00	0·02	0·04	0·06
Fe″	1·98	1·99	1·90	1·77	1·91	1·96	1·50
Mn	0·08	0·20	0·24	0·40	0·32	0·19	0·55
Mg	0·22	0·40	0·24	0·19	0·23	0·11	0·12
Ca	0·73	0·37	0·65	0·72	0·54	0·77	0·90
Si + R‴ + Ti	4·99	5·08	4·98	4·95	4·99	4·99	4·98
R″	3·01	2·96	3·03	3·08	3·00	3·03	3·07
Mol % end members							
Alm.	65·8	67·2	62·7	57·4	63·6	64·7	48·8
Sp.	2·7	6·8	7·9	13·0	10·7	6·3	17·9
Py.	7·3	13·5	7·9	6·2	7·7	3·6	3·9
Gro.	22·2	9·5	19·5	23·4	17·3	24·1	27·4
And.	2·0	3·0	2·0	0·0	0·7	1·3	2·0
Measured optical and physical properties							
n (±0·002)	1·799	1·802	1·798	1·796	1·801	1·802	1·796
a Å (±0·002)	11·611	11·565	11·606	11·613	11·593	11·617	11·642
D (gm/cc)	4·067	4·09	4·085	4·07	4·106	4·086	4·10
	±0·003	±0·01	±0·003	±0·01	±0·003	±0·005	±0·01
Calculated optical and physical properties							
n	1·798	1·803	1·799	1·796	1·802	1·800	1·793
a Å	11·60	11·55	11·59	11·61	11·58	11·61	11·63
D (gm/cc)	4·09	4·14	4·10	4·09	4·12	4·11	4·07

Chemistry. Chemical analyses of seven garnets (table IV) show them to be essentially almandines with significant grossular contents and relatively small spessartine and pyrope components. Compositional variation clearly depends on chemistry of the host rocks. For example,

the grossular content of G10, from a clinopyroxene-bearing rock with 11 wt % CaO, is substantially higher than that in G16, from a rock containing orthopyroxene and 7 wt % CaO. The high grossular content (averaging 20 mol %) of garnets in Willyama rocks of basic affinity contrasts with the virtual absence of this component in almandines from isogradal lime-poor pelitic gneisses. Content of pyrope increases significantly from Zone A to Zone C, but no definite relationship with metamorphic grade can be established from the limited data available because of the effects of variations in rock chemistry and mineralogy.

Small deficiencies in silicon are apparent in the cation contents listed in table IV. These are not thought to result from analytical error, since they would require omissions of up to one weight per cent. of SiO_2. The standard procedure of precipitating silica twice during analysis and of recovering it from pyrosulphate fusions is unlikely to introduce so large an error. If the deficiency is made up with aluminium, the sum of the remaining aluminium, ferric iron, and titanium then closely approximates the ideal 2·00 for the R''' group. As there is insufficient titanium, it is not clear how charge deficiencies resulting from replacement of silicon by aluminium are balanced.

Plagioclase

The following ranges, based on universal stage determinations (method of Turner, 1947) or on partial analyses for alkalis and lime (table V), indicate no systematic differences in plagioclase composition between metabasic rocks or their garnetiferous associates from the three metamorphic zones of the Willyama Complex: Zone A, An_{40}–An_{93}; Zone B, An_{50}–An_{90}; Zone C, An_{33}–An_{88}. In every zone bytownite is the most abundant plagioclase, reflecting the comparatively low sodium contents of parent rocks (typically 1 to 2 wt % Na_2O, cf. Binns, 1964, table II).

The average modal plagioclase content of Zone A and Zone B amphibolites is 25 %, but this increases to 40 % in Zone C basic gneisses. Reversed zoning of plagioclase occurs in about one-third of the specimens examined from Zone C, about one-fifth of those from Zone B, and rarely in Zone A. Zoned grains consist of two parts joined by a narrow transitional zone; relatively homogenous sodic cores and similarly homogenous but more calcic rims. The cores are usually small, and they differ in composition from the rims by about 5 mol % An in Zone B and 10 mol % An in Zone C. The zoning and the increase in abundance

TABLE V. Partial analyses and properties of Willyama plagioclases. Analyst: R. A. Binns. Alkalis determined by flame photometer, lime by EDTA titration, and iron colorimetrically. Some samples are contaminated with quartz. The term 'equivalent feldspar' is the wt % feldspar content of the sample calculated from the analytical figures for alkalis and lime. Two different density fractions of plagioclases P3 and P12 were analysed

		Zone C										
Wt %		P1	P2	P3a	P3b	P4	P5	P6	P7	P8	P10	P11	P12a
Na_2O		3·54	2·00	6·98	2·58	3·10	1·57	5·03	5·08	2·10	2·43	4·88	7·23
K_2O		0·04	0·04	0·19	0·10	0·04	0·04	0·14	0·31	0·05	0·04	0·04	0·21
CaO		13·93	16·47	6·77	2·31	15·06	17·14	11·40	10·50	16·45	15·20	11·48	7·92
Fe_2O_3*		n.d.	0·25	n.d.	n.d.	0·22	n.d.	0·28	n.d.	n.d.	n.d.	0·17	n.d.
Equivalent feldspar		99·4	98·9	93·7	33·8	101·1	98·6	100·0	96·8	99·7	96·2	99·2	101·5
Mol %	Ab	31·4	18·0	64·3	65·8	27·2	14·2	44·0	45·9	18·7	22·4	43·4	61·6
	Or	0·3	0·3	1·1	1·6	0·2	0·3	0·8	1·8	0·3	0·3	0·3	1·1
	An	68·3	81·7	34·6	32·6	72·6	85·5	55·2	52·3	81·0	77·3	56·3	37·3
$2V_\gamma(\pm 2°)$				96			100		77			80	93
$(2\theta_{131}-2\theta_{1\bar{3}1})$ Cu-K_α				1·75°			2·21					1·87	1·78
†	Γ			0·43°			1·37	0·58				0·69	0·47
	B			0·89°			0·76	0·89				0·84	0·90

* Total iron expressed as Fe_2O_3. † $\Gamma = 2\theta_{131}+2\theta_{220}-4\theta_{1\bar{3}1}$ (Cu-K_α) $B = 2\theta_{1\bar{1}1}-2\theta_{\bar{2}01}$ (Cu-K_α).

TABLE V (*cont.*)

	Zone C			Zone B					Zone A		
Wt %	P12b	P16	P18	P26	P27	P28	P29	P30	P34	P36	P37
Na_2O	7·25	2·77	4·36	2·09	2·77	2·06	1·92	3·42	0·93	0·69	1·27
K_2O	0·16	0·06	0·20	0·08	0·10	0·08	0·08	0·05	0·13	0·07	0·04
CaO	7·90	15·31	12·53	16·58	14·75	16·43	16·75	14·41	18·74	15·97	17·22
Fe_2O_3*	n.d.	0·39	0·27	0·16	n.d.	n.d.	n.d.	0·20	n.d.	n.d.	n.d.
Equivalent feldspar	101·4	99·7	100·2	100·3	97·2	98·9	99·7	100·9	101·4	85·5	96·5
Mol % Ab	61·9	24·6	38·2	18·4	25·2	18·4	17·0	29·9	8·2	7·2	11·8
Mol % Or	0·8	0·4	1·1	0·4	0·6	0·4	0·4	0·3	0·7	0·5	0·2
Mol % An	37·3	75·0	60·7	81·2	74·2	81·2	82·6	69·8	91·1	92·3	88·0
$2V_\gamma$ ($\pm 2°$)		93									
$(2\theta_{131}-2\theta_{1\bar{3}1})$ Cu-K_α									2·25°		
† Γ									1·43°		
† B									0·76°		

* Total iron expressed as Fe_2O_3. † $\Gamma = 2\theta_{131}+2\theta_{220}-4\theta_{1\bar{3}1}$ (Cu-K_α) $B = 2\theta_{1\bar{1}1}-2\theta_{\bar{2}01}$ (Cu-K_α).

of plagioclase from Zone B to Zone C may be attributed to grade-dependent breakdown of coexisting hornblendes (cf. Binns 1964).

The water-clear Willyama plagioclases are well-twinned in a multiple fashion on the albite law. Pericline twins and combined albite–Carlsbad twins are also relatively common. Manebach and albite–ala-B twins have been encountered in exceptionally calcic plagioclases (An_{85}–An_{93}) from Zone A. Antiperthitic structures, although prominent in plagioclases from some other granulite facies metabasic rocks (cf. Eskola, 1952), have not been observed in the potash-poor Willyama plagioclases.

Optic axial angles and the functions B and Γ (determined from X-ray diffractometer patterns, following Smith and Gay, 1958) indicate that Zone C plagioclases have structural states intermediate between those of synthetic plagioclases and natural plagioclases from plutonic igneous rocks (fig. 6). Their intermediate character is also apparent from 131–$1\bar{3}1$ spacings plotted on fig. 1 of Slemmons (1962). The high anorthite contents of analysed plagioclases from Zones A and B hinder determination of their structural states by optical or X-ray powder methods.

Although a few specimens retain traces of doleritic or gabbroic texture, most Willyama metabasic rocks have been entirely recrystallized. The abundance and nature of the twinning displayed by their metamorphic plagioclases conflict with the observations of Turner (1951) and Gorai (1951), who contend that twin-laws other than albite and pericline are restricted to igneous rocks. However, the complex twinning might reflect overall calcic composition or be in some way associated with structural state. To the writer's knowledge intermediate structural states have not before been reported for a group of isogradal metamorphic plagioclase feldspars. Complicated twinning was described in plagioclases from Madras charnockitic rocks and from Saxon granulites by Howie (1955), who also listed optic axial angles for the former that suggest intermediate structural states.

Iron-titanium oxide minerals

Magnetite is a comparatively rare mineral in Willyama metabasic rocks, occurring in only six of the thirty-one specimens examined with a reflecting microscope. Ilmenite, however, is ubiquitous. Sulphide minerals are scarce and mostly of secondary origin. The opaque oxide minerals are slightly smaller than coexisting silicates and apart from specimen 10, where magnetite tends to be clustered near poikiloblastic garnets, are evenly distributed through the rocks.

Partial chemical analyses of ten ilmenites and four magnetites are

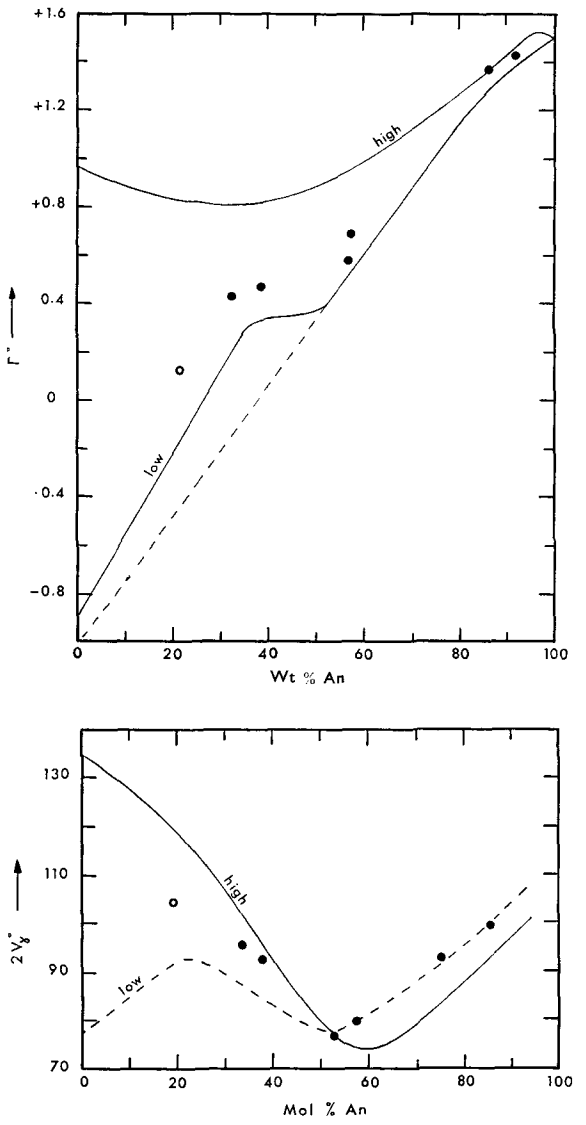

FIG. 6. Plots of optic axial angles (following Smith, 1958) and

$$\Gamma = (2\theta_{131} + 2\theta_{220} - 4\theta_{1\bar{3}1})\ \text{Cu-}K_\alpha$$

(following Smith and Gay, 1958) against composition for Zone C Willyama plagioclases, showing their intermediate structural character. The open circle represents the plagioclase in a Zone C quartzo-feldspathic gneiss and solid circles denote plagioclases listed in table V.

listed in tables VI and VII. The analysed concentrates vary from 95 % to 99·5 % pure. Total iron, titanium, and manganese were determined from pyrosulphate fusions. Separate portions were used for determination of ferrous iron by the ammonium metavanadate method. Care was taken to minimize attack of the silicate impurities, especially garnet, by ceasing pyrosulphate fusions and vanadate solutions immediately the opaque oxides were completely dissolved.

Ilmenite. In polished sections Willyama ilmenites are salmon pink in colour and strongly anisotropic. They show no twinning. Some ilmenites coexisting with magnetite contain tiny (0001) platelets of exsolved hematite, but most are homogenous.

The partial analyses reveal substantial manganese contents (up to 2·70 wt % in I26, which coexists with garnet). In I6, I10, and I26 there are distinct excesses of titania (see fig. 7) that seem unlikely to be due to analytical error or impurities. Buddington and Lindsley (1964) observed that such excesses can be compensated by undetermined constituents, e.g. MgO and CaO.

Compositions based on the $20\bar{2}4$ and $11\bar{2}6$ lattice spacings of ilmenites and their exsolved hematite lamellae (following Lindsley, 1963) are listed in table VI. Since the effects of manganese and other components are not known, little absolute significance can be attached to the values given, but there is a clear relative compositional difference between homogenous ilmenites and the host phases of ilmenites possessing exsolved hematite. The latter apparently contain more hematite in solid solution.

Magnetite. All Willyama magnetites examined contain (111) exsolution lamellae of ilmenite. Cell dimensions of the host magnetite phases (table VII) correspond closely to those of pure Fe_3O_4, suggesting that most of the titanium revealed by analysis is situated in the octahedral ilmenite lamellae. There are no optical or X-ray indications of exsolved ulvöspinel phases. The magnetites in several specimens are altered to hematite along margins or cracks and near ilmenite lamellae. This is probably a secondary feature associated with retrograde metamorphism.

Two of the analysed magnetites listed in table VII (Mt6 and Mt10) have suffered alteration, and only their titanium contents are significant. Despite their possession of ilmenite lamellae, the magnetites Mt3 and Mt18 (the unaltered two) plot close to the magnetite–ulvöspinel join on fig. 7, suggesting that exsolution of ilmenite has not been accompanied by overall oxidation. However, more accurate chemical

TABLE VI. Partial chemical analyses of Willyama ilmenites. Analyst: R. A. Binns

		Zone C							Zone B	
Wt %		I3	I5	I6	I7	I10	I12	I16	I18	I26	I27
TiO_2		51·3	50·8	53·2	48·9	52·0	51·0	46·2	45·4	50·6	52·2
Fe_2O_3		3·1	0·5	6·1	3·8	10·9	4·5	4·8	3·2	3·9	2·5
FeO		44·4	43·5	39·4	41·1	36·5	43·6	42·7	44·9	36·1	41·7
MnO		1·06	0·46	1·18	1·37	0·29	1·25	0·72	0·52	2·70	1·06
Total		99·9	95·3	99·9	95·2	99·7	100·4	94·4	94·0	93·3	97·5
Mol %	FeO*	48·9	48·9	44·6	48·2	41·5	48·4	49·8	51·8	45·1	47·1
	Fe_2O_3	1·5	0·3	3·0	1·9	5·5	2·2	2·5	1·6	2·0	1·3
	TiO_2	49·6	50·8	52·4	49·9	53·0	49·4	47·7	46·6	52·9	51·6
d spacings (Å) of host ilmenite and exsolved hematite lamellae											
host											
d_{204}		1·8669	1·8661	1·8644	1·8657	1·8620	1·8664	1·8668	1·8668	—	1·8661
d_{116}		1·7242	1·7232	1·7220	1·7230	1·7197	1·7239	1·7247	1·7241	—	1·7241
Mol % ilm.‡		98·5	96·5	91·5	95·0	85·0	97·5	98·5	97·5	—	97·0
lamellae											
d_{204}		—	—	1·8450	†	1·8450	—	†	1·8432	—	—
Mol % ilm.		—	—	20	—	20	—	—	11	—	—

* Includes MnO.

† Indicates existence of a small peak due to lamellae of hematite.

‡ Composition in terms of ilmenite–hematite solid solution (see text).

analyses on material of higher purity would be necessary to substantiate this suggestion, which appears unlikely in view of experimental studies of ilmenite exsolution from magnetite–ulvöspinel mixtures (Buddington and Lindsley, 1964).

TABLE VII. Partial chemical analyses and cell dimensions of Willyama magnetites (Zone C). Analyst: R. A. Binns

Wt %		Mt3	Mt6*	Mt10*	Mt18
TiO_2		8·7	5·7	4·3	3·8
Fe_2O_3		52·6	63·8	74·1	58·6
FeO		36·5	26·9	16·9	33·6
MnO		0·20	0·16	0·03	0·03
Total		98·0	96·6	95·3	96·0
Mol %	FeO	53·9	44·4	31·2	53·1
	Fe_2O_3	34·7	47·1	61·6	41·5
	TiO_2	11·4	8·5	7·2	5·4
Cell dimensions of host phase					
a†		8·394 Å	8·391	8·391	8·395

* Partly altered to hematite. † All ±0·002.

The manganese contents of the magnetites are low compared to those of coexisting ilmenites; except for the slightly discrepant pair I3–Mt3, distribution of manganese between Willyama ilmenites and magnetites corresponds to that observed for metamorphic associations by Buddington and Lindsley (1964, fig. 12).

Lindsley (1963, see also Buddington and Lindsley, 1964) has constructed a diagram, based on experimental studies of coexisting magnetite–ulvöspinel and ilmenite–hematite mixtures, from which both temperature and oxygen fugacity during formation can be estimated by using the compositions of coexisting iron–titanium oxides. Willyama pairs I3–Mt3 and I18–Mt18 indicate temperatures of 670° and 600° C respectively and oxidizing conditions comparable to the fayalite–magnetite–quartz buffer assemblage.[1] Although the temperatures compare favourably with those obtained for some Adirondack granulite-facies gneisses by Buddington and Lindsley, they are significantly lower than temperature estimates for Zone C in the Willyama Complex based on amphibole and muscovite breakdown experiments, viz. 750°–850° C (Binns, 1964).

[1] Since ilmenite I18 is slightly deficient in TiO_2 it was necessary to assume that all Fe_2O_3 in the analysis was present as dissolved hematite before exsolution.

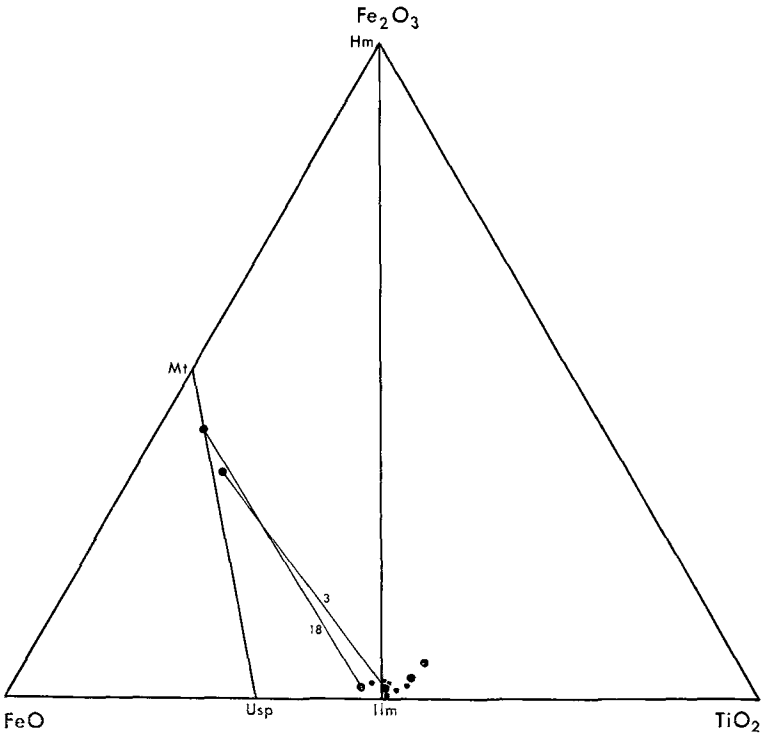

FIG. 7. Triangular plot (mol % FeO, Fe_2O_3, TiO_2) illustrating compositions of Willyama iron–titanium oxide minerals. Ilmenites coexisting with magnetite are denoted by larger symbols than those occurring alone. Tie-lines are shown for pairs I3–Mt3 and I18–Mt18.

Acknowledgements. This work was undertaken at the Department of Mineralogy and Petrology, Cambridge, during tenure of a G.H.S. and I. R. Lightoller Scholarship (University of Sydney) and a Rouse Ball Research Studentship (Trinity College, Cambridge). Dr. P. Gay, Dr. I. D. Muir, Dr. S. R. Nockolds, and Prof. J. F. G. Wilkinson are thanked for much helpful discussion.

References

ATLAS (L.), 1952. Journ. Geol., vol. 60, p. 125 [M.A. **12**–80].
BEST (M. G.), 1963. Journ. Petr., vol. 4, p. 223.
BINNS (R. A.), 1962. Min. Mag., vol. 33, p. 320 [M.A. **16**–190].
——, 1964. Journ. Geol. Soc. Aust., vol. 11, p. 283.
——, 1965. Min. Mag., vol. 35, p. 306.
——, LONG (J. V. P.), and REED (S. J. B.), 1963. Nature, vol. 198, p. 777.
BOWEN (N. L.) and SCHAIRER (J. F.), 1935. Amer. Journ. Sci., ser. 5, vol. 29, p. 151 [M.A. **6**–352].
BOWN (M. G.) and GAY (P.), 1959. Amer. Min., vol. 44, p. 592 [M.A. **14**–418].
—— and ——, 1960. Min. Mag., vol. 32, p. 379 [M.A. **14**–506].

BOYD (F. R.) and ENGLAND (J. L.), 1960. Ann. Rept. Geophys. Lab., Yearbook 59, p. 49.
—— and SCHAIRER (J. F.), 1964. Journ. Petr., vol. 5, p. 275.
BROWN (G. M.), 1956. Phil. Trans. Roy. Soc., ser. B, vol. 240, p. 1 [M.A. **14**–69].
——, 1957. Min. Mag., vol. 31, p. 511 [M.A. **13**–554].
BUDDINGTON (A. F.) and LINDSLEY (D. H.), 1964. Journ. Petr., vol. 5, p. 310.
CLAVAN (W.), MCNABB (W. M.), and WATSON (E. H.), 1954. Amer. Min., vol. 39, p. 566 [M.A. **12**–420].
DAVIS (B. T. C.), 1963. Ann. Rept. Geophys. Lab., Yearbook 62, p. 103.
ENGEL (A. E. J.), ENGEL (C.), and HAVENS (R. G.), 1964. Journ. Geol., vol. 72, p. 131.
ESKOLA (P.), 1952. Amer. Journ. Sci., Bowen vol., p. 133 [M.A. **12**–152].
——, 1957. Madras Univ. Journ., ser. B, vol. 27, p. 101 [M.A. **14**–427].
GORAI (M.), 1951. Amer. Min., vol. 36, p. 884 [M.A. **11**–489].
GREEN (D. H.), 1964. Journ. Petr., vol. 5, p. 134.
HENRY (N. F. M.), 1938. Min. Mag., vol. 25, p. 23.
HESS (H. H.), 1949. Amer. Min., vol. 34, p. 621 [M.A. **11**–15].
——, 1952. Amer. Journ. Sci., Bowen vol., p. 173 [M.A. **12**–97].
——, 1960. Geol. Soc. Amer., Mem. 80 [M.A. **14**–460].
HOWIE (R. A.), 1955. Trans. Roy. Soc. Edin., vol. 62, p. 725 [M.A. **13**–351].
——, 1958. Service Géol. Congo Belge, Bull. 8, fasc. 2 [M.A. **14**–154].
——, 1963. Min. Soc. Amer., Special Paper No. 1, p. 213.
——, 1964a. Min. Mag., vol. 33, p. 903 [M.A. **16**–653].
——, 1964b. Geol. Soc. India, Krishnan vol. (in press).
KRANCK (S. H.), 1961. Journ. Petr., vol. 2, p. 137 [M.A. **16**–564].
LINDSLEY (D. H.), 1963. Ann. Rept. Geophys. Lab., Yearbook 62, p. 60.
MCDOUGALL (I.), 1961. Amer. Min., vol. 46, p. 661 [M.A. **15**–466].
MUIR (I. D.), 1954. Min. Mag., vol. 30, p. 376.
O'HARA (M. J.), 1960. Geol. Mag., vol. 97, p. 145 [M.A. **15**–153].
——, 1961. Journ. Petr., vol. 2, p. 248.
PARRAS (K.), 1958. Bull. Comm. Géol. Finlande, No. 181 [M.A. **14**–306].
PHILIPSBORN (H.), 1930. Chemie der Erde, vol. 5, p. 233 [M.A. **4**–392].
SKINNER (B. J.), 1956. Amer. Min., vol. 41, p. 428 [M.A. **13**–537].
SLEMMONS (D. B.), 1962. Norsk Geol. Tidsskr., Bd. 42, 2 Halvbind, p. 533 [M.A. **16**–464].
SMITH (J. R.), 1958. Amer. Min., vol. 43, p. 1179 [M.A. **14**–284].
SMITH (J. V.), and GAY (P.), 1958. Min. Mag., vol. 31, p. 744.
SUBRAMANIAM (A. P.), 1962. Geol. Soc. Amer., Buddington vol., p. 21 [M.A. **16**–295].
TURNER (F. J.), 1947. Amer. Min., vol. 32, p. 389.
——, 1951. *Ibid.*, vol. 36, p. 581 [M.A. **11**–388].
WILSON (A. D.), 1955. Bull. Geol. Surv. Great Britain, No. 9, p. 56 [M.A. **13**–257].

[*Manuscript received 14 June 1965*]

EXPLANATION OF PLATES

PLATE VIII. *a*. Photomicrograph of clinopyroxene grain from a Zone C basic gneiss showing two sets of exsolution lamellae: (001) clinohypersthene lamellae in a restricted area just right of centre, and (100) orthopyroxene lamellae over most of the grain. The apparent thickness of lamellae in both sets is exaggerated by their non-vertical inclination. Specimen 84323 (C5), crossed nicols, × 160.

b. Photomicrograph of orthopyroxene grain containing (100) exsolution lamellae of clinopyroxene. The host is almost at extinction, one set of lamellae showing

bright interference colours appears as white lines and the other set (with 'twin-like arrangement' to the first) is at extinction and is not clearly visible. Specimen 84323 (O5), crossed nicols, × 100.

PLATE IX. *a*. Photomicrograph of the grain of clinopyroxene C5 studied with the electron probe micro-analyser showing well developed (001) exsolution lamellae of clinohypersthene. Inclined nicols, × 320.

b. Portion of a *c*-axis oscillation photograph of clinopyroxene C5. At the centre of oscillation the X-ray beam was set parallel to the *b* axis. Subsidiary spots due to hypersthene lamellae lie on the same layer lines as intense reflections from the host, but those due to clinohypersthene occur on inclined layer lines below those of the host (cf. Bown and Gay, 1959, fig. 4). Filtered Fe radiation, 30·0 mm radius cylindrical camera.

Note added in proof. Fine antiperthitic exsolution lamellae have recently been reported in some Willyama plagioclases by R. H. Vernon (Min. Mag., vol. 35, p. 505, 1965).

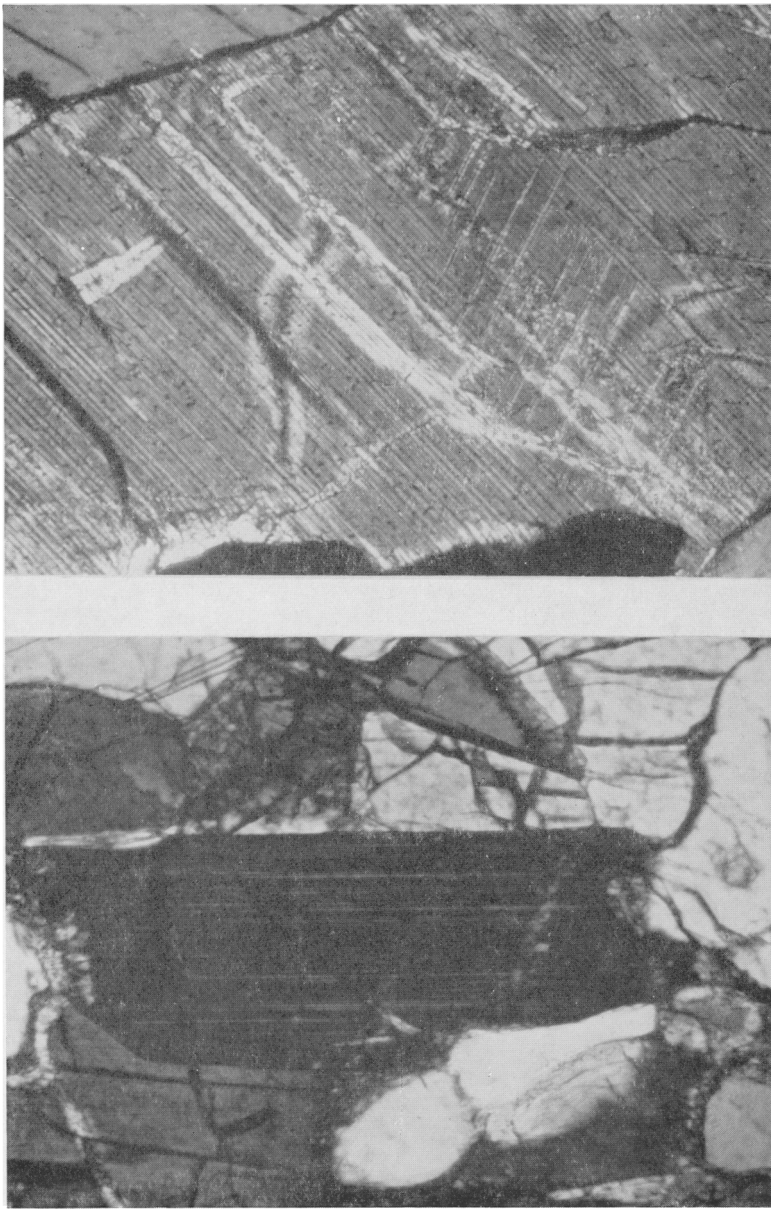

A

B

R. A. BINNS: WILLYAMA METAMORPHIC COMPLEX MINERALS

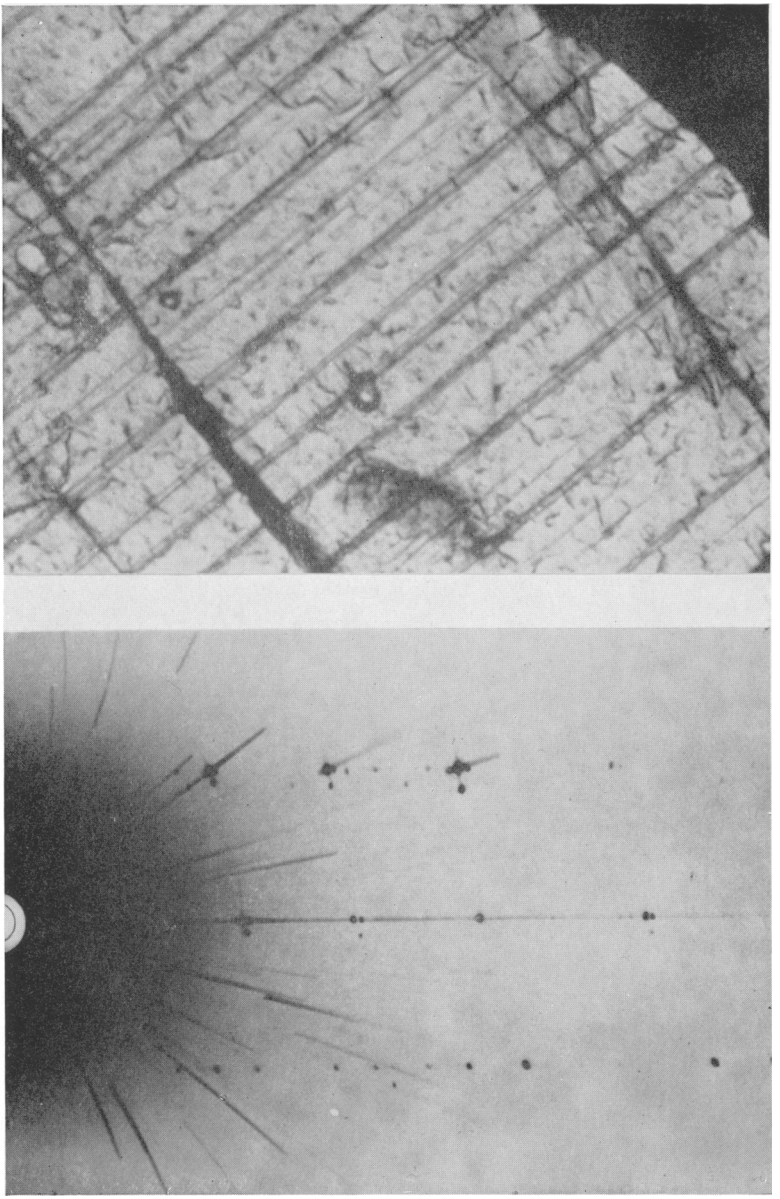

A

B

R. A. BINNS: WILLYAMA METAMORPHIC COMPLEX MINERALS